

Article

Rainfall Monitoring Based on Next-Generation Millimeter-Wave Backhaul Technologies in a Dense Urban Environment

Congzheng Han ^{1,2,*} , Juan Huo ^{1,2}, Qingquan Gao ¹, Guiyang Su ³ and Hao Wang ^{1,2}

¹ Key Laboratory of Middle Atmosphere and Global Environment Observation, Institute of Atmospheric Physics, Chinese Academy of Sciences, Beijing 100029, China; huojuan@mail.iap.ac.cn (J.H.); gqq54515@126.com (Q.G.); wanghao114@mails.ucas.ac.cn (H.W.)

² University of Chinese Academy of Sciences, Beijing 100049, China

³ Zhejiang Provincial Meteorological Observatory, Hangzhou 310002, China; sgy52401314@126.com

* Correspondence: c.han@mail.iap.ac.cn

Received: 31 January 2020; Accepted: 17 March 2020; Published: 24 March 2020



Abstract: High-resolution and accurate rainfall monitoring is of great importance to many applications, including meteorology, hydrology, and flood monitoring. In recent years, microwave backhaul links from wireless communication networks have been suggested for rainfall monitoring purposes, complementing the existing monitoring systems. With the advances in microwave technology, new microwave backhaul solutions have been proposed and applied for 5G networks. Examples of the latest microwave technology include E-band (71–76 and 81–86 GHz) links, multi-band boosters, and line-of-sight multiple-input multiple-output (LOS-MIMO) backhaul links. They all rely on millimeter-wave (mmWave) technology, which is the fastest small-cell backhaul solution. In this paper, we will study the rain attenuation characteristics of these new microwave backhaul techniques at different mmWave frequencies and link lengths. We will also study the potential of using these new microwave solutions for rainfall monitoring. Preliminary results indicate that all the test mmWave links can be very effective for estimating the path-averaged rain rates. The correlation between the mmWave link measurement-derived rain rate and the local rain gauge is in the range of 0.8 to 0.9, showing a great potential to use these links for precipitation and flood monitoring in urban areas.

Keywords: rainfall monitoring; remote sensing; rain rate estimation; 5G; millimeter-wave; E-band; LOS-MIMO

1. Introduction

Accurate and continuous monitoring of rainfall is very important in many applications. While measurements equipment such as satellites, radar, and weather stations are commonly used for rainfall monitoring, other opportunistic sources for relevant data are being exploited as we are living in the era of big data [1,2]. Big data research is pushing the boundaries of these new technologies and analytic tools, and one such important technology for providing weather data is the use of existing physical measurements in wireless microwave signals, such as the signal level in commercial cellular communication networks for near-ground rainfall monitoring [3]. Microwave backhaul links are used for communications between cellular base stations, and can also be used for measuring the path-averaged rain rate. Utilizing microwave backhaul links for environmental monitoring has also been recently mentioned as one of the Internet of Things (IoT) applications [4]. The densely deployed microwave links all of the world have great potential to be used to complement existing monitoring systems.

In the telecommunications industry, to meet the ever increasing demand in consumer data traffic, many countries have already started the deployment of 5G networks. Microwave backhauling is widely used in many frequency bands above 6 GHz and will also remain an essential medium for transport of 5G, in addition to fiber for macro radio deployments. Forty percent of backhaul connections are expected to be based on microwave by 2023, as reported in [5].

The radio spectrum is a scarce resource that is governed by national and international regulations. Operation of 5G networks requires enormous transmission capacity and ultra-low transmission latency [6], which bring great challenges to microwave transmission links [5]. Lower frequencies allow signals to transmit over longer distances and penetrate buildings better. At higher frequencies, signals have limited coverage, however because of much wider bandwidths they can achieve high capacity. The millimeter-wave (mmWave) technology ranging from 30 to 300 GHz is the key to enabling fast speed and high capacity backhauling in future wireless networks [7].

Governments around the world have allowed operations in the millimeter bands for backhauling, often for little or no licensing fee. Traditional backhaul communications are typically used throughout the 6–42 GHz frequency bands, but they are becoming increasingly popular at various mmWave frequency bands in the 50 GHz, 60 GHz, E-band (71–76 and 81–86 GHz), and 92–95 GHz bands throughout the world [8,9]. Even higher frequencies may be of interest to support the evolution of mobile broadband backhauling beyond 2020, such as 92–114.5 (W-band) and 141–174.8 GHz (D-band) frequency ranges [10,11].

A typical cellular network covers a large area and includes conditions ranging from urban canyons to open rural land. Depend on population density and propagation characteristics, geographical land is classified into one of four categories: dense urban, urban, suburban, and rural. For 5G networks, backhaul links in different frequency bands are adopted for different environments to achieve high capacity [5]. For densely populated areas (categorized as “dense urban”), the E-band (70 or 80 GHz) is favorable for links over a few kilometers and offering high capacity in the 10 Gbps band. The W-band (92–114.5 GHz) and D-band (130–174.7 GHz) are currently under investigation and high millimeter frequency bands will be able to support 40 Gbps capacity over about a kilometer range. Microwave links for urban environments typically have short distances and high capacity demand. An E-band link is suitable in these scenarios. In suburban areas, the link length increases and capacity is lower compared to dense urban and urban areas. Traditional bands (e.g., 6 to 42 GHz), multi-carrier, and multi-band, (mid-band, 15–23 GHz) with E-band solutions can be deployed. The range is typically 8 km. For rural environments, the link length increases further, while end site capacity decreases. For these environments, the traditional microwave band is preferred. The range is typically around 15 km. In this article, examples of several latest microwave technologies, including E-band (71–76 and 81–86 GHz) links, line-of-sight multiple-input multiple-output (LOS-MIMO) backhaul links, and multi-band solutions, are investigated.

E-band can provide double the 5 GHz bandwidth, offering a 10 GHz aggregate spectrum (71–76 and 81–86 GHz), enabling Gbps data rates. An 1.4-km long E-band link, which was tested by Ericsson and Deutsche Telekom, has demonstrated a data transmission rate of 40 Gbps, with a round-trip latency performance of less than 100 ms [12]. This is about four times greater data throughput compared to current mmWave backhaul links. The outdoor small cell E-band backhaul links can be rapidly deployed everywhere, including street lamps, rooftops, and the sides of buildings. E-band is becoming an essential backhauling band with high global alignment, which is also expected to facilitate dense mmWave 5G deployments on street-level sites. However, signals in mmWave frequencies are known to suffer from large propagation loss and rain attenuation is one of the main limiting factors [13,14]. As a result, the E-band links are used for high capacity transmission but at shorter distances compared to traditional bands, and can generally be applied to lengths of up to 3 km.

The emerging concept of carrier aggregation enables a much more efficient use of diverse backhaul spectrum assets. As it is easier to obtain wider channels at higher frequencies, we can aggregate a low frequency carrier for availability and a high frequency carrier for capacity. A multi-band solution

combining E-band with traditional bands can increase the transmission distance. The traditional band links are used to guarantee the availability of high-priority services and support transmission distances of 3 to 10 km. This will allow the use of E-band to provide transmission for 5G in much wider geographical areas. A commonly used combination is 18–42 GHz bands and E-band (70 or 80 GHz) for distances up to 5 km (dense urban and urban environments), and 6–15 and 18–42 GHz bands for longer transmission ranges (suburban and rural environments). In this article, we will study the impact of atmospheric conditions on E-band backhaul links in city environments, especially rain attenuation. A 38 GHz mmWave backhaul link deployed in the same region will also be studied for comparison analysis.

The different forms of antenna technology refer to single or multiple inputs and outputs. When there are more than one antenna at the transmit side and receive side of the radio link, this is referred to as a multiple-input multiple-output (MIMO) system. MIMO can be used to provide improvements in both channel robustness and channel throughput compared to a single-input single-output (SISO) system, where there is a single antenna at the transmit side and receive side of the radio link [15,16]. MIMO has been widely used in wireless local area networks (WLANs), long-term evolution (LTE) mobile networks, and fifth generation cellular systems. MIMO with a spatial multiplexing scheme allows capacity to increase almost linearly with the number of antennas. Recently, MIMO technology has been applied to increase transmission rates in point-to-point backhaul links in mmWave bands for next-generation wireless backhaul networks [17–20]. This is referred to as a line-of-sight multi-input multi-output (LOS-MIMO) communication system. Most existing studies of the impact of rain on signal attenuation are for SISO microwave links. Signal attenuation in a MIMO backhaul link due to rain and other meteorological conditions are yet to be studied.

Large signal attenuation can occur due to heavy rain and can severely affect the mmWave link quality. Modeling and measurements of mmWave attenuation due to rainfall for near-ground communication links have been addressed in recent studies and are considered very important topics [21–26]. A power law empirical mathematical model relating the rain rate and rain-induced signal attenuation is given by International Telecommunication Union (ITU) Recommendation P. 838-3 and other relevant papers [27–29]. This model is used in the design of reliable communication systems. Recently, it has been suggested that microwave links in cellular networks can be considered as passive weather monitoring sensors, and a power law model relating the rain and rain attenuation can be adopted for rainfall estimation [30–32]. This approach exploits the fact that the strength of electromagnetic signals is weakened by certain weather conditions, especially rain. It makes microwave linking a potential tool for monitoring rainfall conditions with high temporal and spatial resolution. There is significant potential to increase the number of observation points and improve the quality of weather services, including forecasting, now-casting, flood warnings, and hydrological measurements. The most powerful impact is expected in developing countries and regions where no other measurements currently exist. Making use of the existing commercial wireless networks is equivalent to deploying a very high density of weather monitoring sensors and forming wireless environmental sensor networks (WESN) [30,33] all over the world.

The major contributions in this paper are (1) studying and comparing the rain attenuation characteristics of latest mmWave backhaul links and (2) studying the performance of rain rate estimation based on SISO and MIMO links at different frequencies, using existing measurements of the received signal level of the mmWave backhaul links.

This paper is organized as follows. Section 2 presents a brief summary of characteristics of mmWave propagation, the method of rain rate retrieval from the received signal level of mmWave links, and the setup of outdoor test links. Section 3 presents the experimental results on signal variation in sunny and rainy weather, wet antenna effects and the performance of rain rate retrieval studies using the latest mmWave backhaul test links. Then, the uncertainties in the experiment and the potentials of the proposed technology in supporting rainfall and flood monitoring in urban areas are discussed in Section 4. Finally, we summarize the work in Section 5.

2. Materials and Methods

2.1. Millimeter-Wave Propagation

For a point-to-point LOS mmWave link, the received power P_B (dBm) may be related to the transmitted power P_T (dBm); the antenna gains G_T (dBi) and G_R (dBi); and the propagation path loss (PL), atmospheric loss (AL) and other losses (OL). The link can be written as:

$$P_B = P_T + G_T + G_R - PL - AL - OL \quad (1)$$

The propagation path loss can be expressed as [34]:

$$PL(f_c, d) = 32.4 + 20\log_{10}(f_c) + 10n\log_{10}(d/d_0) + \chi_\sigma, d \geq 1m \quad (2)$$

where f_c denotes the carrier frequency in GHz, d is the transmitter and receiver separation distance, the reference distance d_0 is 1 m, and n represents the path loss exponent. Here, χ_σ is a zero-mean Gaussian random variable with a standard deviation σ in dB.

2.2. LOS-MIMO-Based mmWave Backhaul System

The principle of a 2×2 LOS-MIMO microwave backhaul link is to design a MIMO channel with a phase difference of 90 degrees between short and long paths to make the signal streams orthogonal to each other. The channel is denoted by a $N \times M$ matrix \mathbf{H} , and each element represents the channel from the m th transmit (Tx) antenna to the receive (Rx) antenna n th. Note that $N = M = 2$ in our measurement setup. Each element of the channel matrix can be written as $H_{mn} = e^{j\theta_{mn}}$, where θ_{mn} is the phase of the sub-channel. For the phase of the sub-channel from the n th transmit antenna to the m th receive antenna, $\theta_{mn} = 2\pi r_{mn}/\lambda$, where λ is the wavelength and r_{mn} is the propagation distance between the transmit antenna n and receive antenna m [19,20]. This can be achieved by designing the antenna separation distance at the transmitter d_1 and receiver d_2 to fulfill, $d_1 \times d_2 = \lambda L/N$, where L is the path length between the transmit site and receive site. Let \mathbf{X} and \mathbf{Y} denote the transmit and receive signal vector, respectively. The $N \times 1$ received signal vector can be written as:

$$\mathbf{Y} = \sqrt{P_R}\mathbf{H}\mathbf{X} + \mathbf{W}$$

$$\begin{bmatrix} Y_1 \\ Y_2 \end{bmatrix} = \sqrt{P_R} \begin{bmatrix} H_{11} & H_{12} \\ H_{21} & H_{22} \end{bmatrix} \begin{bmatrix} X_{A1} \\ X_{A2} \end{bmatrix} + \begin{bmatrix} W_1 \\ W_2 \end{bmatrix} \quad (3)$$

where \mathbf{W} is the $N \times 1$ complex additive white Gaussian noise vector and its variance equals N_0 ; P_R is the average received power, expressed in watts, where $P_R = 10^{P_B/10}$.

In practice, a sub-optimal linear zero-forcing algorithm can be applied to simply invert the channel and independently decode the data streams at the receiver to recover the spatially multiplexed signals:

$$\mathbf{G} = P_R^{-1/2}\mathbf{H}^+ = P_R^{-1/2}(\mathbf{H}^H\mathbf{H})^{-1}\mathbf{H}^H \quad (4)$$

The character $^+$ denotes the pseudo-inverse operation. By applying the pseudo-inverse of the channel matrix to the received signal we get:

$$\begin{aligned} \tilde{\mathbf{X}} &= \mathbf{G}(P_R^{1/2}\mathbf{H}\mathbf{X} + \mathbf{W}) = \mathbf{X} + \mathbf{G}\mathbf{W} \\ &= \mathbf{X} + P_R^{-1/2}\mathbf{H}^+\mathbf{W} \end{aligned} \quad (5)$$

The SNR after interference cancellation for the i th sub-channel is given as:

$$SNR_i = \frac{P_R}{N_0 \left[(\mathbf{H}^H\mathbf{H})^{-1} \right]_{i,i}} \quad (6)$$

Here, $\left[\left(\mathbf{H}^H\mathbf{H}\right)^{-1}\right]_{i,i}$ refers to the (i, i) th elements of $\left(\mathbf{H}^H\mathbf{H}\right)^{-1}$. The independent and identical (i.i.d) MIMO channel capacity, assuming equal transmit power, is given as:

$$C = \sum_{i=1}^N \log_2(1 + SNR_i) \quad (7)$$

where $(\cdot)^H$ denotes the Hermitian transpose.

2.3. Atmospheric Attenuation

Atmospheric attenuation and weather effects are important for mmWave propagation. The atmospheric loss is generally defined in terms of decibel (dB) loss per kilometer of propagation. Since the fraction of the signal loss is a strong function of the distance travelled, the actual signal loss experienced by a specific mmWave link due to atmospheric effects depends directly on the length of the link. A simple model describing the attenuation of mmWave for the range of 1 to 100 GHz through atmosphere AL can be described as follows:

$$AL = A_r + A_v + A_o + A_p \text{ (dB)} \quad (8)$$

which primarily includes the attenuation effects of dry air (including oxygen), humidity, fog, and rain. Here, A_r refers to the attenuation caused by rain, A_v represents the water vapor attenuation, A_o represents the attenuation due to dry air, and A_p is the attenuation as a result of other-than-rain precipitation (i.e., fog, sleet, snow).

There are other possible causes of losses (OL), such as the coaxial cable loss at the transmitter and receiver; temperature and water vapor affecting the stability of the transmit and receive signal terminals (equipment, circuits, etc.); wetness of the transmit and receive antenna surface causing considerable attenuation; and anything that obstructs the LOS channel introducing additional loss.

2.3.1. Water Vapor Attenuation

Attenuation due to absorption by oxygen and water vapor is always present and should be included in the calculation of total propagation loss at frequencies above approximately 10 GHz. For the millimeter frequency range, the resonance lines for water vapor and oxygen are at 22.3, 183.3, 323.8 GHz; and 57–63 and 118.74 GHz, respectively.

To illustrate the electromagnetic signal attenuation due to dry air and water vapor, Figure 1 was plotted based on the equations given in [35], for a given barometric pressure and temperature. The first excess attenuation occurs at around 22 GHz due to water vapor, and the second at 60 GHz due to oxygen. Oxygen absorption has a maximum attenuation at 60 GHz and contributes to 7–15 dB/km in the received signal strength at the frequency range of 57–63 GHz. For 32 and 38 GHz, the signal is mainly affected by water vapor, and the attenuation is less than 0.15 dB for a 1 km link length. For signals in E-band, the attenuation due to humidity can reach approximately 0.5 dB/km [24,35].

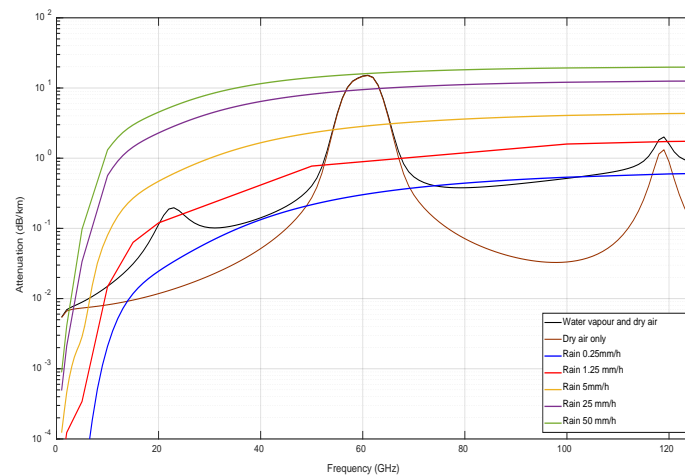


Figure 1. Frequency-dependent attenuation of electromagnetic radiation in standard atmosphere (barometric pressure 1013 mbar, temperature 15 °C, water vapor density of 7.5 g/m³) and rain attenuation in dB/km at various rainfall rates.

2.3.2. Rainfall Effects on Radio Signals

A power law empirical model is often used in the calculation of rain-induced attenuation A_r and the average rain rate R [28,29] along the path:

$$A_r = aR^b L \text{ (dB)} \quad (9)$$

where the constants a and b are related to frequency, rain temperature, the rain drop size distribution, and polarization, depending on the rain attenuation model. In our study, L (km) is the length of the microwave link and A_r is the overall signal attenuation induced by rain between the transmitter and receiver. A set of commonly used power law coefficients can be found in International Telecommunication Union (ITU) Recommendation P. 838-3 [28]. The power law coefficients for vertical polarization (a_V , b_V) and horizontal polarization (a_H , b_H) at different frequencies are summarized in Table 1. Assuming vertical polarization, the power law coefficients a and b used in our measurement are given in Table 1.

Table 1. Power law coefficients for different frequencies.

Frequency	a_H	a_V	b_H	b_V	a	b
32 GHz	0.2778	0.2646	0.9302	0.8981	0.2646	0.8981
38 GHz	0.4001	0.3844	0.8816	0.8552	0.3844	0.8552
72 GHz	1.0618	1.0561	0.7293	0.7171	1.0561	0.7171
82 GHz	1.1946	1.1915	0.7077	0.6988	1.1915	0.6988

The rain attenuation values for the considered millimeter frequency band in this study at various rainfall rates (R) are given in Table 2. We categorized the rainfall intensity into six groups, including very light rain (rain rate < 1 mm/h), light rain (1 mm/h ≤ rain rate < 2 mm/h), moderate rain (2 mm/h ≤ rain rate < 5 mm/h), heavy rain (5 mm/h ≤ rain rate < 10 mm/h), very heavy rain (10 mm/h ≤ rain rate < 20 mm/h), extreme heavy rain (rain rate ≥ 20 mm/h). The theoretical rain-induced signal attenuation per kilometer based on Equation (9) for our considered millimeter frequencies is presented in Figure 2a. Compared to other atmospheric factors, atmospheric attenuation due to rain is one of the most noticeable components of excess losses at our considered frequencies. It is not important for low frequency bands, but rain affects links in millimeter frequency ranges, especially for higher frequencies. For increasing rain rate, the rain attenuation experienced by E-band links becomes more severe compared to the 32 and 38 GHz links. For a very heavy rain event, the rain-induced signal

attenuation can be up to 9.7 dB for the 82 GHz link at a rain intensity of 20 mm/h. Figure 2b gives the theoretical rain attenuation for our measurement setup. Both 32 and 38 GHz links are 7-km long, and both 72 and 82 GHz are 3 km long. Based on the power law coefficients given by ITU-R P. 838-3, a 7-km long 38 GHz link experiences similar or less signal attenuation compared to a 3 km E-band link for rain intensity lower than 7 mm/h. At 32 GHz, the rain attenuation is lower compared to an E-band signal, even if the link has more than double the deployment length.

Table 2. Signal loss due to rain (dB/km).

Description	Rain Rate (mm/h)	Signal Loss (dB) Per Kilometer			
		32 GHz	38 GHz	72 GHz	82 GHz
Very light rain	$R < 1$	< 0.3	< 0.4	< 1.1	< 1.2
Light rain	$1 \leq R < 2$	< 0.5	< 0.7	< 1.7	< 1.9
Moderate rain	$2 \leq R < 5$	< 1.1	< 1.5	< 3.3	< 3.7
Heavy rain	$5 \leq R < 10$	< 2.1	< 2.75	< 5.5	< 6.0
Very heavy rain	$10 \leq R < 20$	< 3.9	< 5.0	< 9.1	< 9.7
Extreme rain	$R \geq 20$ (e.g., 50)	≥ 3.8 (8.9)	≥ 5.0 (10.9)	≥ 9.1 (17.5)	≥ 9.7 (18.3)

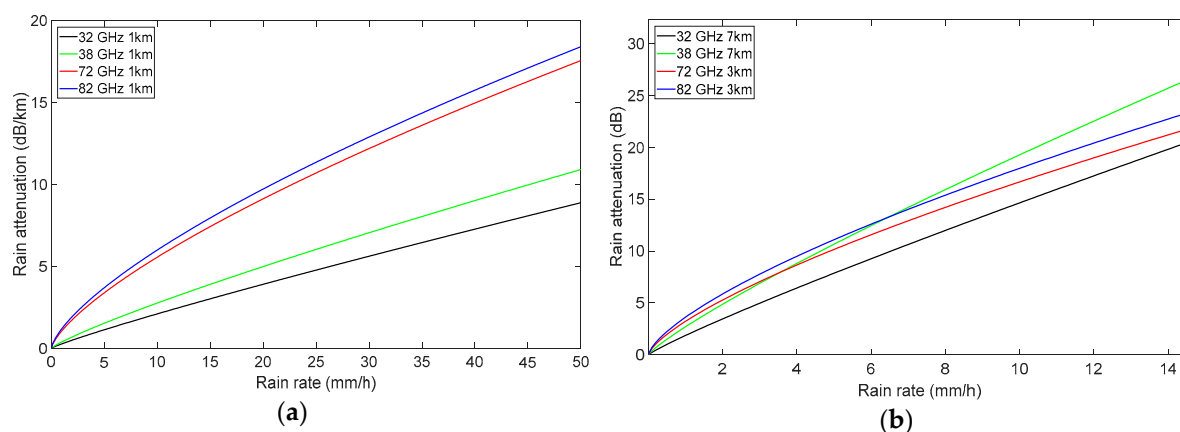


Figure 2. The theoretical rain-induced signal attenuation for various rain rates at different frequencies: (a) per kilometer; (b) over a 7-km long 32 GHz 2×2 line-of-sight multiple-input multiple-output (LOS-MIMO) link, a 7-km long single-input single-output (SISO) 38 GHz link, a 3-km long 72 GHz link, and a 3-km long 82 GHz test link using our measurement scenario.

2.3.3. Rain Rate Estimation Using the Receive Signal Levels from Millimeter-Wave Links

The use of microwave links for near-ground environmental monitoring is a new technology, and it has shown to be an effective tool for rainfall monitoring in over 20 countries. The method of retrieving the rain rate from the rain-induced attenuation in the received signal level is based on the power law model in Equation (9) from the recommendations of the ITU-R P. 838-3:

$$R = \sqrt[b]{\frac{A_r}{aL}} \quad (\text{mm/h}) \quad (10)$$

For a vertical polarized setup, the power law coefficients a and b for the frequencies considered in this study are presented in Table 1, derived from [28]. Therefore, the average rain rate along a link can be derived from the microwave link rain-induced attenuation. In order to determine the signal attenuation caused by rain, we will need to choose a reference level P_{ref} , which can be calculated using the average of the received power in the previous 3 hours in dry weather before rain [36,37]. If there are I observations, then the rain attenuation for the i th observation becomes:

$$A_{r,i} = P_{ref} - P_{R,i} \quad (11)$$

For the case of the LOS-MIMO system, we assume that link length L is the same for all MIMO data streams.

2.4. Outdoor Measurement

We present here a summary of the measurements from three outdoor test mmWave links and local rainfall measurements using rain gauges. These measurements are also used to validate the accuracy of rain rate estimation.

The locations of the three test links are illustrated in Figure 3. The measurement setup parameters are given in Table 3. The transmitter and the receiver of the 32 GHz LOS-MIMO link and the 38 GHz link were closely installed between site A and B. Both links had a length of approximately 6.87 km. One side of the two links was on the roof of the Ericsson building (site A), close to water. Both the 32 GHz LOS-MIMO link and 38 GHz SISO link were operated in a line-of-sight environment. The 32 GHz LOS-MIMO link was horizontally deployed, with antenna separation at both sites. The antenna separation at one end (site B) was fixed and installed at 5 m, whereas antennas at the other end (site A) were installed on tripods, with an antenna separation distance of 7.93 m. The details of the measurement setup can be found in [38]. Here, the radio link operating in the forward transmission direction is referred to as link 1, while the radio link operating in the opposite transmission direction is referred to as link 2. The 32 GHz LOS-MIMO link employed 2 antennas at both the transmit and receive sides, while 2 data streams were transmitted in the forward direction and in the opposite direction over the radio link. Altogether, 4 data streams were in transmission simultaneously. Note that the data used in this study from the LOS-MIMO test link is recorded at the receiver without post-processing, but for practical deployment, the received data streams should be decoupled using carrier-to-interference (C/I) measurement. Since the rain attenuation is mainly distance dependent as shown in Equation (9), the actual wanted and interference signal power will not impact on the accuracy of rain retrieval analysis.

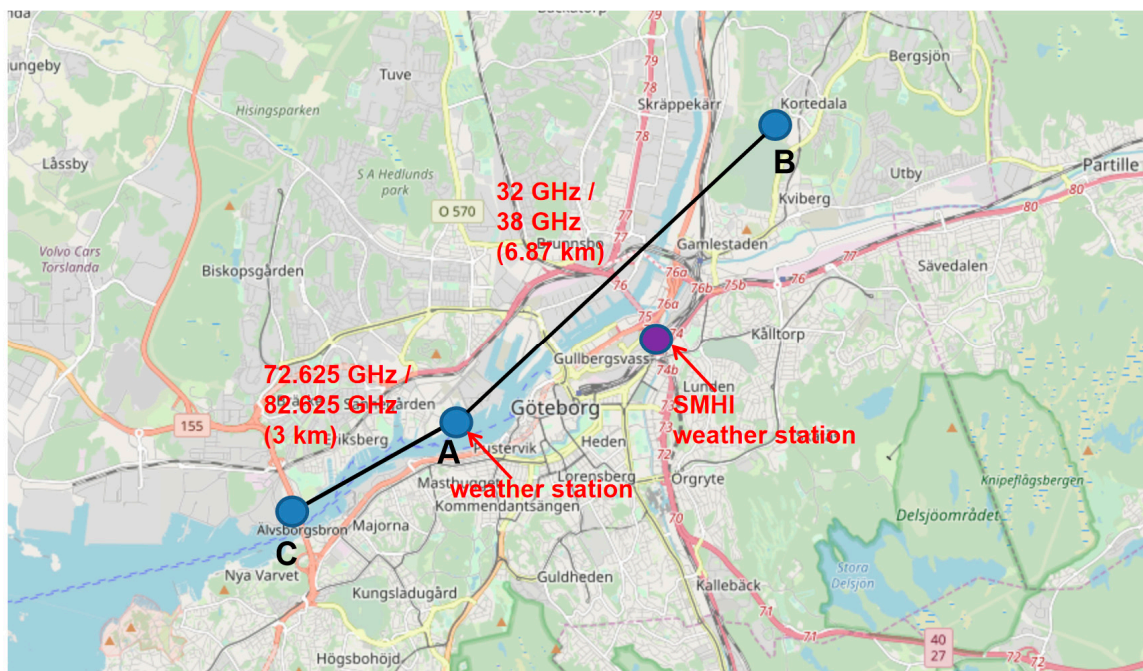


Figure 3. The measurement setup and locations in Gothenburgh, Sweden. SMHI, Swedish Meteorological and Hydrological Institute.

Table 3. Outdoor measurement parameters.

Parameter	32 GHz	38 GHz	72.625 GHz	82.625 GHz
Sampling interval	30 s			
Antenna type	Cassegrain antenna			
Location	57°42′18.97″ N, 11°56′29.67″ E; 57°44′52.8″ N, 12°1′26.4″ E		57°42′18.97″ N, 11°56′29.67″ E; 57°41′20.04″ N, 11°54′10.76″ E	
Link length	6.87 km		3 km	
Setup	MIMO	SISO	SISO	SISO
Antenna no.	2 × 2	1 × 1	1 × 1	1 × 1
Antenna Separation	5 m; 7.93 m	N/A	N/A	N/A
Tx power	5 dBm	15 dBm	7 dBm	7 dBm
Tx antenna gain	43.6 dBi	40.3 dBi	50.5 dBi	50.5 dBi
Tx half power beam width	0.5°	0.5°	0.5°	0.5°
Tx polarization	V	V	V	V
Rx antenna gain	43.6 dBi	40.3 dBi	50.5 dBi	50.5 dBi
Rx half power beam width	0.5°	0.5°	0.5°	0.5°
Rx polarization	V	V	V	V

For the 38 GHz SISO link, one data stream was transmitted in the forward and reverse directions, and there were 2 data streams transmitting instantaneously over the radio link.

For the 3 km SISO E-band link, one end was also installed on the roof of the Ericsson building at site A and was deployed between sites A and C. The geographic locations of the E-band links are listed in Table 3. In the forward transmission the radio link operates at 72.625 GHz, while in the reverse transmission the radio link operates at 82.625 GHz.

All the mmWave links have a sampling interval of 30 seconds. Rain, humidity, temperature, air pressure, and wind information were provided by a weather station equipped with a rain gauge located at the rooftop of the Ericsson building. The accuracy of the rain gauge is of the order $\pm 3\%$ [39]. We used the measurement from this rain gauge for the analysis in the results section. As this weather station was located on the rooftop, we also selected the closest rain gauges operated by the Swedish Meteorological and Hydrological Institute (SMHI). The SMHI rain gauge reported the cumulative rain amount in mm over 1 day and its location is indicated in Figure 3.

3. Measurement Results

During the outdoor trial measurements, the received signal level and path attenuation were recorded in changing weather conditions for the three mmWave links at 32 GHz, 38 GHz, and E-band ranges. All the links were in operation at the same time.

3.1. Rainfall Effects

The received signal variation and the rain intensity on 7 and 11 June 2017 are presented in Figures 4 and 5, respectively. Assuming other losses (wet antenna attenuation, water vapor attenuation, etc.) are the same, the average signal attenuation values over 1 km distance are also compared in Figures 4b and 5b, which show more clearly the impact of rain on links at different frequencies. The measured rain attenuation result is consistent with the theoretical predictions in Table 2. Although the 32 and 38 GHz links were built over a much longer distance compared to the E-band links, the rain-induced attenuation in the 32 and 38 GHz links was lower. This difference in rain-induced attenuation between the lower and higher frequency mmWave link becomes more significant as the rain intensity increases. The 32 GHz and 38 GHz links are more robust to poor weather conditions compared to the E-band link, although they are deployed over longer distances. The attenuation of the links, especially the E-band link, was a lot more severe than expected in late evening on 7 and 11 June. One possible reason is that

the rain gauge provides a point measurement, while the measured signal attenuation is caused by the rain along the link. Although one side of all links is located on top of the same building, the links are built across different and wide areas, with a separation distance of up to 10 km. The rain intensity that each link experienced along the path could be very different from the rain gauge measurement, and it could contribute to the difference in attenuation value. In addition, the rain gauge that was used for the analysis was located on the rooftop of a building. There could be a significant under catch of rainfall in the gauge especially during windy conditions, and more rainfall could have been detected by the mmWave link.

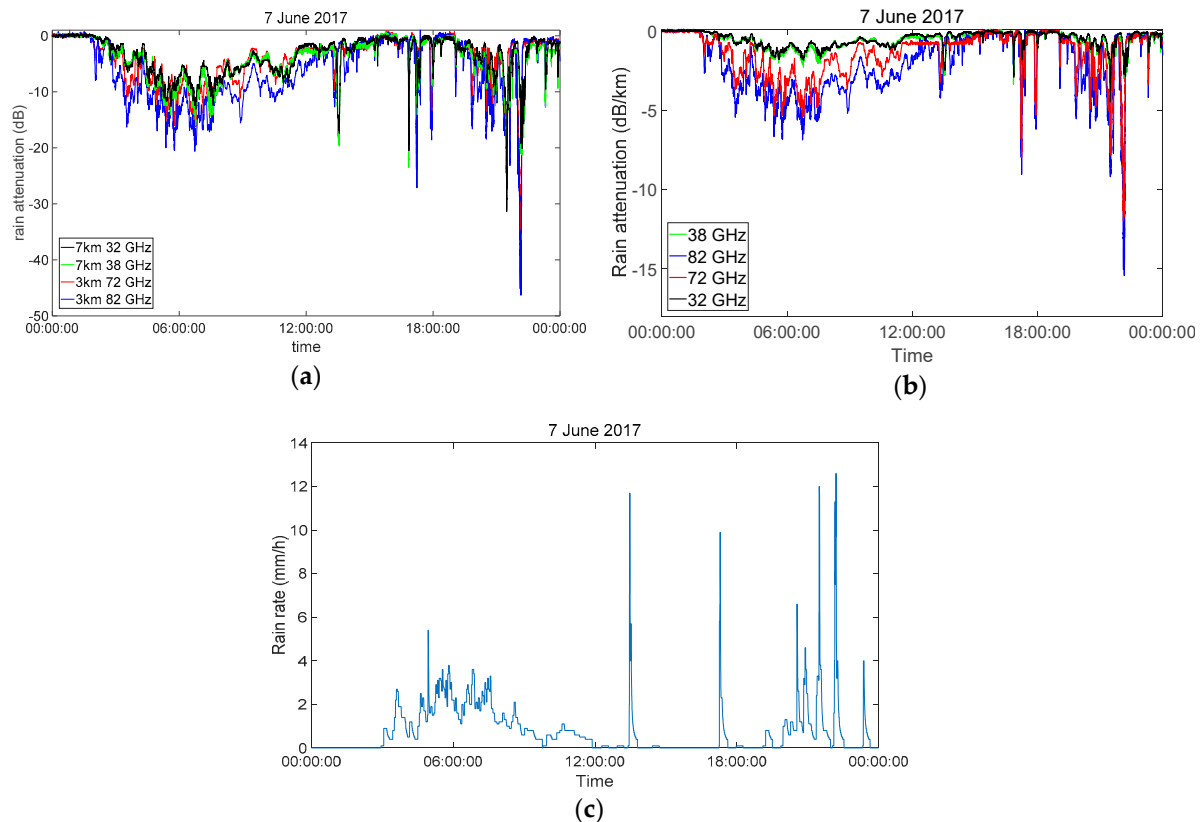


Figure 4. (a) Received signal variation of the test links on June 7, 2017; (b) received signal variation of the test links averaged over 1 km distance; (c) rain rate monitored by a rain gauge.

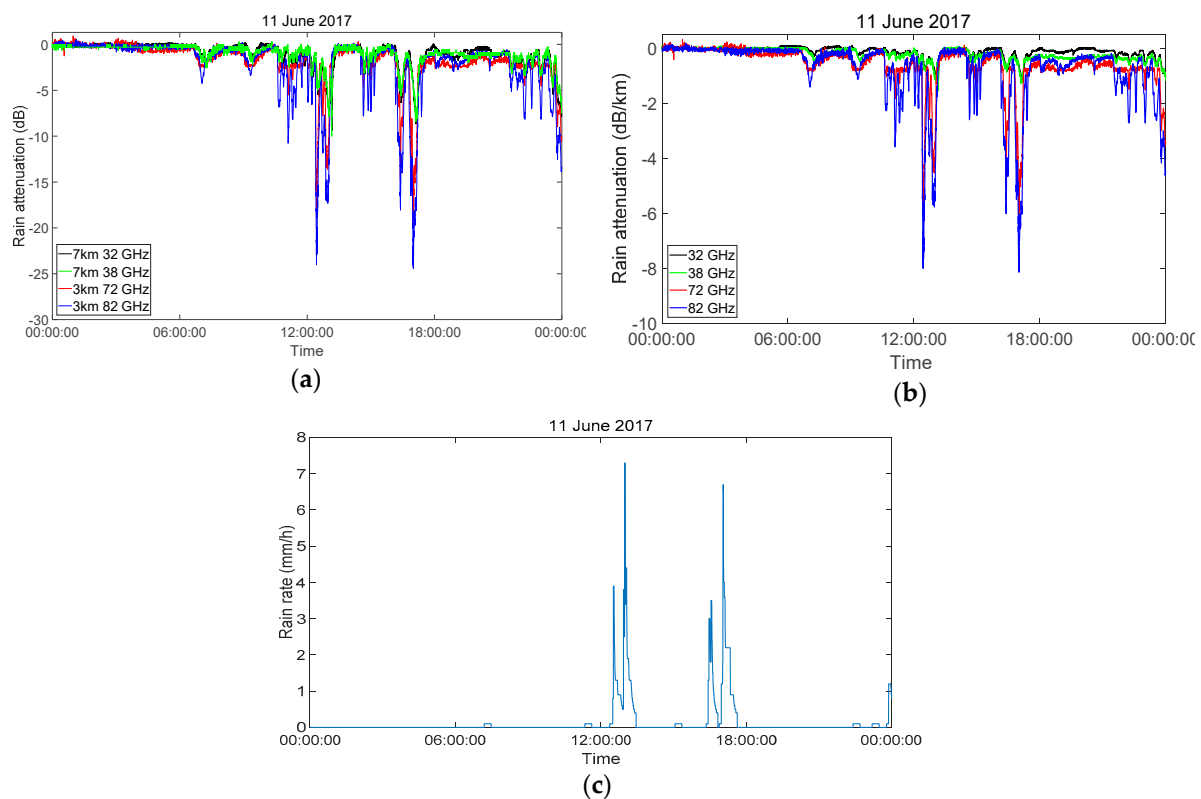


Figure 5. (a) Received signal variation of the test links on June 11, 2017. (b) received signal variation of the test links averaged over 1 km distance. (c) rain rate monitored by a rain gauge.

3.2. Water Vapor Attenuation

As discussed in the previous section, change in water vapor level may also cause additional attenuation. Atmospheric attenuation of signal level due to dry air and water vapor is related to the air pressure, temperature, and the water vapor density. For the dry period from 13 to 15 June 2017, the changes in temperature, air pressure, and humidity level are presented in Figure 6a, and the variations of the received signal level from the test links are also given in Figure 6. During these sunny days, it can be seen that the received signal level also varies over time as a result of atmospheric effects. The variation of temperature and humidity is inversely related with a correlation coefficient of -0.9 . Attenuation from water vapor is a function of the pressure p (hPa), temperature T ($^{\circ}\text{C}$), and the water vapor density ρ (g/m^3) [35]. For the frequencies considered in this study, the signal attenuation due to oxygen absorption is negligible. The attenuation due to changes in water vapor density at 32 and 38 GHz is very low, approximately up to 1 dB for a 7-km long link, as shown in Figure 6b,c. As the frequency increases to the E-band, variation in water vapor density can contribute over 0.45–0.55 dB/km for E-band signals, and therefore a total of 1.35–1.65 dB for the 3 km link, which is illustrated in Figure 6d.

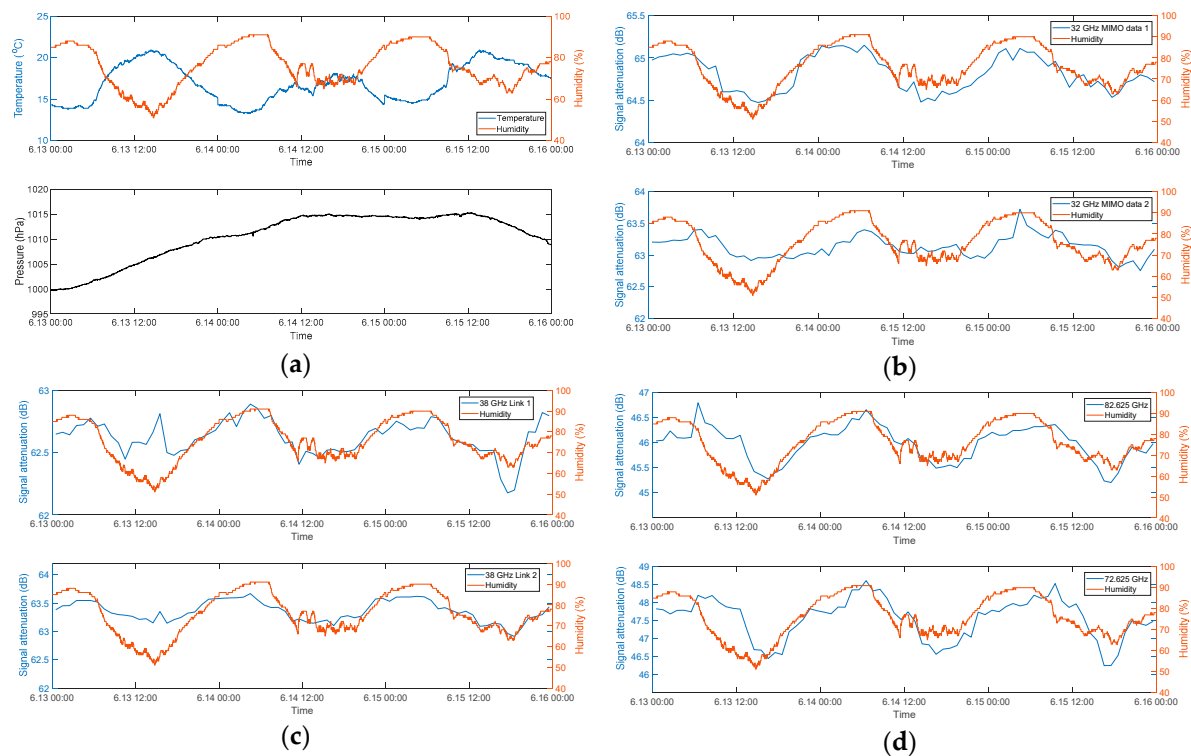


Figure 6. (a) The variations in temperature, humidity, and pressure during 13–15 June, 2017. (b) The variations in the signal attenuation and humidity of the 32 GHz link (link 1, data streams 1 and 2). (c) Links 1 and 2 at 38 GHz; (d) The 72.625 and 82.625 GHz links.

3.3. Data Post-Processing and Uncertainties

The determination of the baseline level and wet antenna attenuation are very important for accurate estimation of rain rates from the mmWave links [40–42]. Here, we consider the reference level to be the average received signal strength over 3 hours in dry weather before rain. Subtracting the baseline level, also called the reference level, from the actual received signal levels gives the rain-induced, path-integrated attenuation, which can be transformed into the path averaged rain rate.

During rainy periods, the dampening of the radomes of the antenna causes attenuation, and this additional attenuation factor is known as the wet antenna effect [40]. The wet antenna effect has been shown to be consistent for a specific microwave link, but varies from link to link. Therefore, it has been suggested that the wet antenna attenuation depends on the specific link properties, such as the signal polarization, frequency, and the radome material, meaning each link needs to be examined individually. For a rainfall event lasting for a long period of time, the wet antenna attenuation is expected to increase with increasing thickness of water film on the antenna. In addition to wet antenna attenuation, water vapor may also cause additional variation at high frequencies, as shown in Section 3.2. As discussed in [41,42], bias due to the instability of the transmit power of commercial microwave backhaul equipment could be up to 1.6 dB, therefore causing more attenuation to the received signal level. Therefore, hardware (radio, antenna) and alignment possibly also contribute to this difference. This could be studied as future work if long term measurement is carried out and analyzed.

For the experiment period, the measured statistics of rain attenuation versus calculated rain attenuation, based on Equation (9), are plotted in Figure 7. Each point represents the rain rate and measured attenuation value from the link measurement over a 15 min interval. The correction factor, which mainly accounts for wet antennas, is applied to the measurement data. As the water vapor attenuation is insignificant, it is combined in one correction factor. The distribution of rain attenuation values for increasing rain rate before and after applying the correction factor is presented.

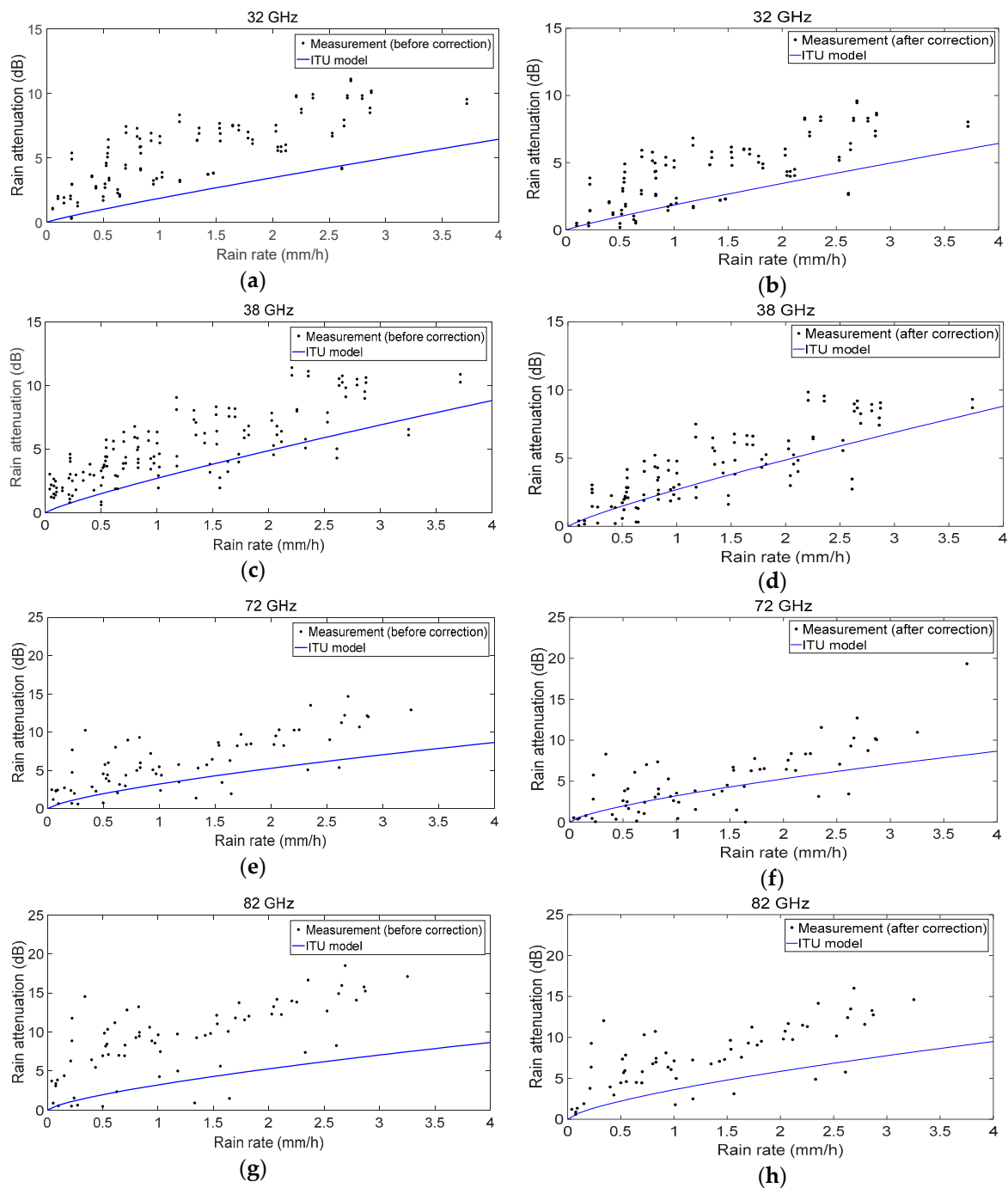


Figure 7. Rain attenuation statistics from the measurement before correction and after correction in comparison with the calculated rain attenuation, using the ITU model from Equation (9) for different frequencies: (a,b) 32 GHz; (c,d) 38 GHz; (e,f) 72 GHz; (g,h) 82 GHz.

3.4. Rain Rate Estimation

We evaluate the rainfall estimates from mmWave test links through three metrics—the Pearson correlation coefficient, the root mean square difference, and the bias.

The linear dependence of the time series data of average rain attenuation obtained from the link measurement $X = A_r$ and rain rate measurement $Y = R$ from the rain gauge is estimated by calculating

the correlation coefficient of the variables. If each variable has I averaged observations, the Pearson correlation coefficient is calculated as:

$$r(A_{r,i}, R_i) = r(X_i, Y_i) = \frac{1}{I-1} \sum_{i=1}^I \left(\frac{X_i - \mu_X}{\sigma_X} \right) \left(\frac{Y_i - \mu_Y}{\sigma_Y} \right) \quad (12)$$

where μ_X and σ_X are the mean and standard deviation of X , respectively, and μ_Y and σ_Y are the mean and standard deviation of Y . Here, r ranges from -1 to $+1$. A high correlation coefficient value shows stronger relation between two data sets. On 7 and 11 June 2017, the signal power attenuation is mainly caused by rainfall and the values are highly correlated, resulting in an average correlation coefficient greater than 0.8. The strong correlation between the receive signal attenuation and rain rate during the measurement period indicates that it is possible to retrieve the rain rate from the receive signals of the mmWave links.

After applying the correction to the signal attenuation, the rain rate is estimated on a 15 min basis using Equation (10). The time series data of average rain rate derived from the mmWave link measurement $X = R_{link}$ is then compared with the rain rate measurement $Y = R$ from rain gauge, based on Equation (12). Figures 8 and 9 show the comparison between the link-derived rain rate estimation and rain gauge measurement. The accuracy of the rain estimation using different links is presented in Table 4. The root mean square difference (RMSD) was also computed for accuracy analysis according to the following formula:

$$RMSD = \sqrt{\frac{1}{I} \sum_{i=1}^I (X_i - Y_i)^2} \quad (mm/h) \quad (13)$$

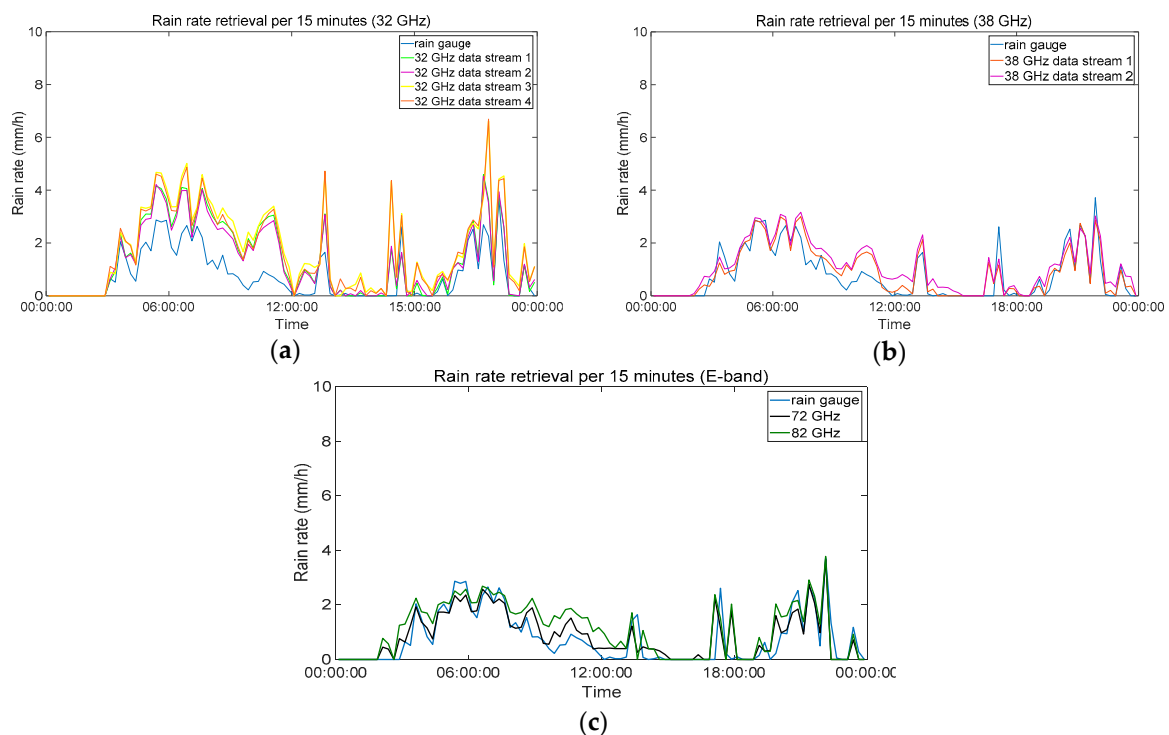


Figure 8. Average rain rate per 15 min derived from the signal link compared with the rain gauge measurement on 7 June 2017: (a) 32 GHz link; (b) 38 GHz link; (c) E-band link.

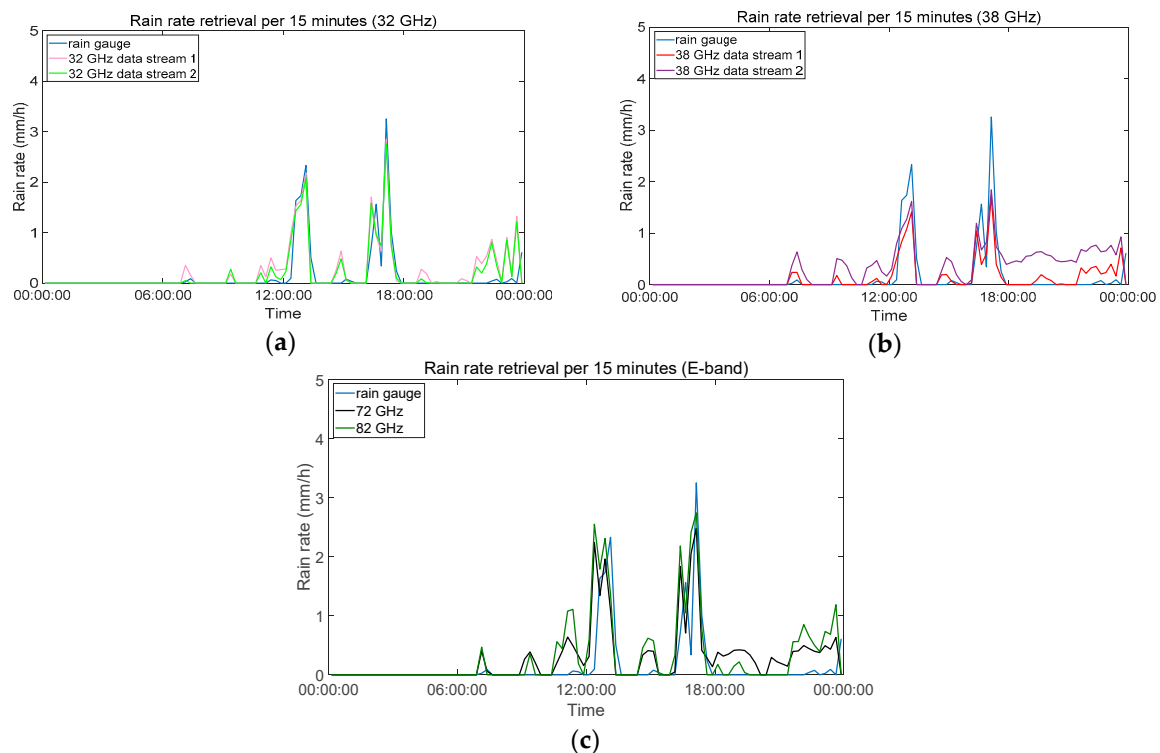


Figure 9. Average rain rate per 15 min derived from the signal link compared with the rain gauge measurement on 11 June 2017: (a) 32 GHz link; (b) 38 GHz link; (c) E-band link.

Table 4. Accuracy analysis of rain retrieval from the three test links.

Frequency	Data Stream	Correction	Correlation	RMSD	BIAS
32 GHz	1 (link 1)	1.5 dB	0.87	0.95	0.60
	2 (link 1)	1.5 dB	0.88	0.84	0.56
	1 (link 2)	1.5 dB	0.84	1.00	0.55
	2 (link 2)	1.5 dB	0.85	0.94	0.49
38 GHz	1 (link 1)	1.0 dB	0.90	0.36	0.06
	1 (link 2)	1.0 dB	0.88	0.48	0.25
73 GHz	1 (link 1)	1.5 dB	0.83	0.48	0.12
83 GHz	1 (link 2)	1.75 dB	0.80	0.61	0.26

The bias is a measure of the average error between the link estimate rain rate and the rain gauge measurements, and it can be calculated using the following formula:

$$Bias = \frac{1}{I} \sum_{i=1}^I (X_i - Y_i) \quad (14)$$

The rain rates derived from the three mmWave links are closely related to the observed rain rate recorded by the weather stations, with a very good accuracy. The RMSD is found to be in the range of 0.36–1.00 mm/h for the test links.

Using the latest introduction of MIMO mmWave links, the number of rain estimation values grows linearly with the minimum number of transmitter and receiver antennas of the MIMO link compared to the case of a single rain rate estimation value from a SISO backhaul link. Both the forward and reverse links can be used for rainfall estimation, and the 4 data streams in 2×2 MIMO links can effectively provide up to 4 rain rate estimation values over the path. All the data streams can contribute to understanding of the statistics of the local rain rates.

4. Discussion

It can be seen from the results that the link-experienced rain attenuation could be much higher than the ITU model [28]-predicted attenuation value calculated using the rain gauge records. One possible reason was the location of the rain gauge. The weather station used in this study was located on the rooftop of a business building. A non-rooftop weather station operated by SMHI near the measurement area is available, but the data was not collected very frequently, making comparison with the microwave link derived rain rate at 15 minutes interval difficult. The daily rainfall amounts recorded by the SMHI rain gauge were 39 and 9 mm on 7 and 11 June, respectively, while the recorded daily rainfall values by the rain gauge used for this study was 17.4 and 7 mm, respectively, during these two days. Compression of atmospheric streamlines will produce significant Bernoulli lifting and cause under catch of rainfall in the rain gauge located on the rooftop. The actual rainfall along the links was greater than the rain gauge measurements, which was also indicated by the bias calculation results. The positive bias values show that the rainfall estimated based on the attenuation of the mmWave link signals is higher than the rain rate recorded by the rain gauge. As expected, the mmWave links detected more rainfall than the rooftop rain gauge, which underestimated the rainfall amount.

The widely deployed microwave links from existing cellular networks have become installation-free facilities, and they can be particularly useful for applications in urban hydrology and in supporting monitoring in flood-prone urban areas. Rain gauges have high accuracy but the measurement data is collected at the point scale. Because of the temporal and spatial variability of rainfall, especially in the heavy rain and flooding events, the changes of rain rate occur at very short time intervals. Even in dense urban areas, the density of rain gauges is often not sufficient to capture significant variation in observed rainfall. Radars and satellites can monitor over much wider areas, but the estimates from those sources are less accurate at near-ground levels, and the temporal and spatial resolution is not sufficient for flood monitoring purposes. The measurements presented here records a received signal level measurement every 30 seconds, producing 10 rain rate estimates within 5 minutes, which is usually the time resolution of weather radars. Microwave backhaul links can measure near-ground rain rates more accurately with high time resolution, which could assist in flash flood warnings [43–45], as the wireless networks exist over large regions of land, including complex topographies, where traditional monitoring equipment cannot be easily installed. Therefore, this technology could also be very useful in cities that lack monitoring of rainfall by radar. As more mmWave links are expected to be widely deployed in cities, those densely deployed links can all be used for rainfall monitoring, and the amount of rainfall estimation data will be impressively large. These links can be further processed using standard interpolation methods to create rainfall maps, or combined with other existing monitoring networks based on radars and rain gauges to produce high temporal and spatial resolution rainfall maps [46].

5. Conclusions

New mmWave technologies, including E-band, multi-band boosters, and LOS-MIMO, have been recently introduced to meet the global demand on microwave backhaul capacity and 5G network build-out. The large bandwidth available at mmWave frequencies in the 30–300 GHz range will enable very high connection speed and capacity. With large available bandwidth, E-bands (71–76 and 81–86 GHz) are considered a strategic solution for 5G heterogeneous networks. While E-band links are generally used up to 3 km, a multi-band technology combining E-band with traditional lower frequency bands is suggested for longer distance deployment. Supporting transmission of multiple data streams simultaneously, LOS-MIMO is the latest wireless backhaul technology to significantly increase the capacity of short-range, point-to-point, mmWave line-of-sight connections. In this paper, these new wireless backhaul technologies are studied using outdoor test links deployed in the same region. The trial was performed in Gothenburgh, Sweden, over the Ericsson premises in 2017.

Real time path attenuation caused by changing weather conditions were monitored and recorded for a 32 GHz 2×2 LOS-MIMO link and a 38 GHz SISO link over 6.87 km, as well as an E-band microwave

backhaul link over 3 km. The measurement records showed that the rain-induced attenuation of all the three test links are closely related to the variation of the rain rate, with an average correlation value greater than 0.8. The 32 GHz LOS-MIMO link and 38 GHz link were deployed in the same location; the rain attenuation was similar for the two links, but the LOS-MIMO has greater capacity compared to a SISO link. While the 32 and 38 GHz links were built over a much longer distance than the E-band link, but they were less affected by atmospheric attenuation. For light rainfall, the difference in the signal attenuation observed in three test links is less significant. As the rain intensity increases, over a relatively short deployment of 3 km, for the 82 GHz link, the rain attenuation could be greater than 40 dB for a heavy rain event. The high rain attenuation restricts the use of E-band links over longer distances. While E-band backhaul links can achieve high throughput, the coverage is limited; lower frequency links are more robust and can be deployed over much longer distances. Multi-band booster technology pairs a higher frequency link with a lower frequency link, meaning the capacity and coverage requirements for the next-generation microwave backhaul links can be met compared to a single frequency microwave link.

Accurate rain monitoring of precipitation is of great importance to many applications, including meteorology, hydrology, agriculture, and flood monitoring. Microwave backhaul link is considered as a new tool for near-ground rainfall monitoring. We examined the accuracy of using these new mmWave backhaul technologies for rain rate estimation. Additional attenuation due to effects of water film on the antenna surface and other atmospheric conditions, such as humidity, needs to be considered for rain rate estimation for improved accuracy. In real deployments, the measured rain attenuation of the test links is found to be 1–1.75 dB higher than calculated rain attenuation based on the ITU model. We have applied data post-processing and attenuation correction to the received signal level measurement. The derived rain rate from all the links have been shown to be very good compared to the rain rate recorded by the weather stations located in the measurement site. These additional weather data obtained from commercial cellular networks will be particularly useful for big data analysis. Furthermore, mmWave backhauls are expected to be widely used for 5G and smart city networks in cities and densely populated areas, and there is a great potential to use these links for precipitation and flood monitoring in urban areas.

Author Contributions: Conceptualization, C.H.; methodology, C.H.; software, C.H.; validation, G.S., H.W.; formal analysis, C.H.; investigation, J.H.; resources, C.H.; data curation, Q.G.; writing—original draft preparation, C.H.; writing—review and editing, C.H.; visualization, C.H.; supervision, C.H.; project administration, J.H.; funding acquisition, C.H. All authors have read and agreed to the published version of the manuscript.

Funding: This research was funded by National Natural Science Foundation of China, grant number 41605122, 41775032; Chinese Academy of Sciences President’s International Fellowship Initiative for Visiting Scientists, grant number 2018VTA0013.

Acknowledgments: The authors would like to thank Ericsson gratefully for giving them access to data. The authors would also like to thank Hagit Messer and Pinhas Alpert’s research groups for helpful advice.

Conflicts of Interest: The authors declare no conflict of interest.

References

- McCabe, M.F.; Rodell, M.; Alsdorf, D.E.; Miralles, D.G.; Uijlenhoet, R.; Wagner, W.; Lucieer, A.; Houborg, R.; Verhoest, N.E.; Franz, T.E.; et al. The future of earth observation in hydrology. *Hydrol. Earth Syst. Sci.* **2017**, *21*, 3879. [[CrossRef](#)] [[PubMed](#)]
- Tauro, F.; Selker, J.; Van De Giesen, N.; Abrate, T.; Uijlenhoet, R.; Porfiri, M.; Manfreda, S.; Caylor, K.; Moramarco, T.; Benveniste, J.; et al. Measurements and observations in the XXI century (MOXXI): Innovation and multi-disciplinarity to sense the hydrological cycle. *Hydrol. Sci. J.* **2018**, *63*, 169–196. [[CrossRef](#)]
- Gazit, L.; Messer, H. Advancements in the statistical study, modeling, and simulation of microwave-links in cellular backhaul networks. *Environments* **2018**, *5*, 75. [[CrossRef](#)]
- Muller, C.L.; Chapman, L.; Johnston, S.; Kidd, C.; Illingworth, S.; Foody, G.; Overeem, A.; Leigh, R.R. Crowdsourcing for climate and atmospheric sciences: Current status and future potential. *Int. J. Climatol.* **2015**, *35*, 3185–3203. [[CrossRef](#)]

5. Ericsson Mobility Report. December 2018. Available online: <https://www.ericsson.com/assets/local/microwave-outlook/documents/ericsson-microwave-outlook-report-2018.pdf> (accessed on 31 January 2020).
6. Ji, B.; Li, Y.; Chen, S.; Han, C.; Li, C.; Hong, W. Secrecy Outage Analysis of UAV Assisted Relay and Antenna Selection for Cognitive Network under Nakagami-m Channel. *IEEE Trans. Cogn. Commun. Netw. Spec. Issue AI-based Licens./Unlicensed Spectr. Interoperability Future Mob. Wirel. Syst.* **2020**, 1–11. [[CrossRef](#)]
7. Dehos, C.; González, J.; Domenico, A.; Kténas, D.; Dussopt, L. Millimeter-wave access and backhauling: The solution to the exponential data traffic increase in 5G mobile communications systems. *IEEE Commun. Mag.* **2014**, *52*, 88–95. [[CrossRef](#)]
8. Studies on Frequency-Related Matters for International Mobile Telecommunications Identification Including Possible Additional Allocations to the Mobile Services on a Primary Basis in Portion(s) of the Frequency Range Between 24.25 and 86 GHz for the Future Development of International Mobile Telecommunications for 2020 and Beyond. Resolution 238 (WRC-15). Available online: https://www.itu.int/dms_pub/itu-r/oth/0c/0a/R0C0A00000C0014PDFE.pdf (accessed on 31 January 2020).
9. Agenda and Reference (Resolutions and Recommendations), ITU. August 2017. Available online: https://www.itu.int/dms_pub/itu-r/oth/14/02/R14020000010001PDFE.pdf (accessed on 31 January 2020).
10. Frequency Band Review for Fixed Wireless Services. Final Report Prepared for Ofcom, Document 2315/FLBR/FRP/3. 2011. Available online: <http://stakeholders.ofcom.org.uk/binaries/consultations/spectrum-review/annexes/report.pdf> (accessed on 31 January 2020).
11. Chen, X. OFDM based multi-node transmission in the presence of phase noises for small cell backhaul. *IEEE Commun. Lett.* **2017**, *21*, 1207–1210. [[CrossRef](#)]
12. Daniels, G. Deutsche Telekom Achieves Fiber-like Results with MmWave Wireless Backhaul for 5G. 11 January 2019. Available online: <https://www.telecomtv.com/content/news/deutsche-telekom-achieves-fiber-like-results-with-mmwave-wireless-backhaul-for-5g-33773/> (accessed on 31 January 2020).
13. Sen, R.; Singh, M.P. Effect of rain on millimeter-wave propagation—A review. *AIP Conf. Proc.* **2007**, *923*, 45–76.
14. Han, C.; Duan, S.; Bao, L.; Zhang, G.; Ji, B.; Ran, L. E-Band Link for Next Generation Small-Cell Backhaul in Dense Urban Environment. In Proceedings of the IEEE VTC 2019 Fall, Honolulu, HI, USA, 22–25 September 2019; pp. 1–2.
15. Han, C.; Harrold, T.; Armour, S.; Krikidis, I.; Videv, S.; Grant, P.M.; Haas, H.; Thompson, J.S.; Ku, I.; Wang, C.-X.; et al. Green radio: Radio techniques to enable energy efficient wireless networks. *IEEE Commun. Mag. Spec. Issue Green Commun.* **2011**, *49*, 46–52. [[CrossRef](#)]
16. Nicolaou, M.; Han, C.; Beh, K.C.; Armour, S.; Doufexi, A. MIMO techniques for green radio guaranteeing QoS. *IEEE J. Commun. Netw. Spec. Issue Green Radio Energy Effic. Wirel. Netw.* **2010**, *12*, 130–139.
17. Sacchi, C.; Rahman, T.F.; Hemadeh, I.A.; El-Hajjar, M. Millimeter-wave transmission for small-cell backhaul in dense urban environment: A solution based on MIMO-OFDM and space-time shift keying (STSK). *IEEE Access* **2017**, *5*, 4000–4017. [[CrossRef](#)]
18. Hansryd, J.; Edstam, J. Microwave capacity evolution. *Ericsson Rev.* **2011**, *88*, 22–27.
19. Rundstedt, K.; Bao, L.; Krishnan, R.; Olsson, B.-E.; Eriksson, T. On Field Measurements and Modelling of 2×2 Microwave LOS-MIMO Systems. In Proceedings of the IEEE Global Communications Conference (GLOBECOM), San Diego, CA, USA, 6–10 December 2015; pp. 1–6.
20. Bøhagen, F.; Orten, P.; Øien, G. optimal design of uniform rectangular antenna arrays for strong line-of-sight MIMO channels. *J. Wirel. Commun. Netw.* **2007**, *2007*, 045084. [[CrossRef](#)]
21. Zhao, Q.; Li, J. Rain attenuation in millimeter wave ranges. In Proceedings of the International Symposium on Antennas, Propagation, & EM Theory, Guilin, China, 26–29 October 2006.
22. Coldrey, M.; Allasia, A.; Bao, L.; Boch, E.; Ferrari, G.; Gentina, D.; Putkonen, J.; Sutton, A.; Yigal, L.; Zein, N. *Maturity and Field Proven Experience of Millimeter Wave Transmission*; ETSI White Paper: Sophia Antipolis, France, 2015.
23. Forknall, N.; Cole, R.; Webb, D. Cumulative Fading and Rainfall Distributions for a 2.1 km, 38 GHz, Vertically Polarized, Line-of-Sight Link. *IEEE Trans. Antennas Propag.* **2008**, *56*, 1085–1093. [[CrossRef](#)]
24. Han, C.; Duan, S. Impact of atmospheric parameters on the propagated signal power of millimeter-wave bands based on real measurement data. *IEEE Access* **2019**, *7*, 113626–113641. [[CrossRef](#)]
25. Niu, Y.; Li, Y.; Jin, D.; Su, L.; Vasilakos, A.V. A survey of millimeter wave (mmWave) communications for 5G: Opportunities and challenges. *Wirel. Netw.* **2015**, *21*, 2657–2676. [[CrossRef](#)]

26. Han, C.; Duan, S. The study on characteristics of rain attenuation along 28 GHz and 38 GHz line-of-sight millimeter-wave links. In Proceedings of the 2019 URSI Asia-Pacific Radio Science Conference (AP-RASC), New Delhi, India, 9–15 March 2019; pp. 1–3.
27. Liebe, H.J.; Hufford, G.A.; Cotton, M.G. Propagation modeling of moist air and suspended water/ice particles at frequencies below 1000GHz. In Proceedings of the Electromagnetic Wave Propagation Panel Symposium, AGARD Conference Proceedings, Palma, Spain, 17–20 May 1993.
28. ITU-R P. 838–3 (International Telecommunication Union Radio Communication Bureau Propagation Recommendation). *Specific Attenuation Model for Rain for Use in Prediction Methods*; ITU-R: Geneva, Switzerland, 2005.
29. Medhurst, R.G. Rainfall attenuation of centimeter waves: Comparison of theory and measurement. *IEEE Trans. Antennas Propag.* **1965**, *13*, 550–564. [[CrossRef](#)]
30. Messer, H. Capitalizing on cellular technology—Opportunities and challenges for near ground weather monitoring. *Environ. Sci. Technol.* **2018**, *5*, 73. [[CrossRef](#)]
31. Uijlenhoet, R.; Overeem, A.; Leijnse, H. Opportunistic remote sensing of rainfall using microwave links from cellular communication networks. *Wiley Interdiscip. Rev. Water* **2018**, *5*, e1289. [[CrossRef](#)]
32. Chwala, C.; Kunstmann, H. Commercial microwave link networks for rainfall observation: Assessment of the current status and future challenges. *Wiley Interdiscip. Rev. Water* **2018**, *6*, e1337. [[CrossRef](#)]
33. Zhang, G.; Han, C.; Ji, B.; Shi, C.; Xie, P.; Yang, L. A new multiple-symbol differential detection strategy for error-floor elimination of IEEE 802.15.4 BPSK receivers impaired by carrier frequency offset. *Wirel. Commun. Mob. Comput.* **2019**, *2019*, 5409612. [[CrossRef](#)]
34. Rappaport, T.S.; Xing, Y.; MacCarney, G.R.; Molisch, A.F.; Mellios, E.; Zhang, J. Overview of millimeter wave communications for fifth-generation (5G) wireless networks—with a focus on propagation models. *IEEE Trans. Antennas Propag.* **2017**, *65*, 6213–6230. [[CrossRef](#)]
35. ITU-R P. 676–10 (International Telecommunication Union Radio communication Bureau Propagation Recommendation). *Attenuation by Atmospheric Gases*; ITU-R: Geneva, Switzerland, 2013.
36. Overeem, A.; Leijnse, H.; Uijlenhoet, R. Retrieval algorithm for rainfall mapping from microwave links in a cellular communication network. *Atmos. Meas. Tech.* **2016**, *9*, 2425. [[CrossRef](#)]
37. Han, C.; Bi, Y.; Duan, S.; Lu, G. Rain rate retrieval test from 25 GHz, 28 GHz, and 38 GHz millimeter-wave link measurement in Beijing. *IEEE J. Sel. Top. Appl. Earth Obs. Remote Sens.* **2019**, *12*, 2835–2847. [[CrossRef](#)]
38. Bao, L.; Olsson, B.-E.; Hansryd, J. On measurements of availability penalty due to antenna separation in a 2 × 2 LOS-MIMO Link. In Proceedings of the EuCAP, London, UK, 9–13 April 2018.
39. Davis Wireless Vantage Pro2 Weather Station 6322. Available online: <https://www.davisnet.com/weather-monitoring/> (accessed on 31 January 2020).
40. Ostrmetzky, J.; Raich, R.; Bao, L.; Hansryd, J.; Messer, H. The wet-antenna effect—A factor to be considered in future communication networks. *IEEE Trans. Antennas Propag.* **2018**, *66*, 315–322. [[CrossRef](#)]
41. Leijnse, H.; Uijlenhoet, R.; Berne, A. Errors and uncertainties in microwave link rainfall estimation explored using drop size measurements and high resolution radar data. *J. Hydrometeorol.* **2010**, *11*, 1330–1344. [[CrossRef](#)]
42. Zinevich, A.; Messer, H.; Alpert, P. Prediction of rainfall intensity measurement errors using commercial microwave communication links. *Atmos. Meas. Tech.* **2010**, *3*, 1385–1402. [[CrossRef](#)]
43. Raich, R.; Alpert, P.; Messer, H. Vertical prediction estimation using microwave links in conjunction with weather radar. *Environments* **2018**, *5*, 74. [[CrossRef](#)]
44. Eshel, A.; Messer, H.; Ostrometzky, J.; Raich, R.; Alpert, P.; Laronne, J.B. On the use of measurements from a commercial microwave link for evaluation of flash floods in arid regions. *Atmos. Chem. Phys. Discuss.* **2017**. [[CrossRef](#)]
45. Hoedjes, J.C.B.; Kooiman, A.; Maathuis, B.H.P.; Said, M.Y.; Becht, R.; Limo, A.; Mumo, M.; Nduhiu-Mathenge, J.; Shaka, A.; Su, B. A conceptual flash flood early warning system for Africa, based on terrestrial microwave links and flash flood guidance. *ISPRT Int. J. Geo-Inf.* **2014**, *3*, 584–598. [[CrossRef](#)]
46. Liberman, Y.; Samuels, R.; Alpert, P.; Messer, H. New algorithm for integration between wireless microwave sensor network and radar for improved rainfall measurement and mapping. *Atmos. Meas. Tech.* **2014**, *7*, 3549–3563. [[CrossRef](#)]



© 2020 by the authors. Licensee MDPI, Basel, Switzerland. This article is an open access article distributed under the terms and conditions of the Creative Commons Attribution (CC BY) license (<http://creativecommons.org/licenses/by/4.0/>).